miR-100 and *miR-125b* Contribute to Enhanced 3D Growth and Invasiveness and can be Functionally Transferred to Silence Target Genes in Recipient Cells

Hannah M. Nelson[1], Shimian Qu[1], Sydney N. Chapman[1], Nicole L. Luthcke[1], Sara A. Schuster[1], Lauren A. Turnbull[1], Muhammad Shameer[1], Lucas L. Guy[1], Xiao Liu[2], Kevin C. Corn[3], Kasey C. Vickers[4], Qi Liu[2], Jeffrey L. Franklin[5], Alissa M. Weaver[6], Marjan Rafat[3], Robert J. Coffey[7], James G. Patton[1*]

[1]Laboratory of James G. Patton, Department of Biological Sciences, Center for Extracellular Vesicle Research, Vanderbilt University, Nashville, TN, United States

[2]Laboratory of Qi Liu, Department of Biostatistics, Department of Biomedical Informatics, Center of Extracellular Vesicle Research, Vanderbilt University Medical Center, Nashville, TN, United States

[3]Laboratory of Marjan Rafat, Department of Biomedical Engineering, Department of Chemical and Biomolecular Engineering, Department of Radiation Oncology, Vanderbilt University, Nashville, TN, United States.

[4]Laboratory of Kasey C. Vickers, Department of Pathology, Microbiology and Immunology, Department of Medicine, Department of Molecular Physiology and Biophysics, Center for Extracellular Vesicle Research, Vanderbilt University Medical Center, Nashville, TN, United States.

[5]Department of Cell and Developmental Biology, Center for Extracellular Vesicle Research, Vanderbilt University, Vanderbilt University Medical Center, Nashville, TN, United States.

[6]Laboratory of Alissa M. Weaver, Department of Cell and Developmental Biology, Department of Pathology, Microbiology and Immunology, Center for Extracellular Vesicle Research, Vanderbilt University Medical Center, Nashville. TN, United States.

[7]Laboratory of Robert J. Coffey, Department of Medicine, Division of Gastroenterology, Hepatology and Nutrition, Department of Cancer Research, Department of Cell and Developmental Biology, Center for Extracellular Research, Vanderbilt University Medical Center, Nashville, TN, United States.

[*]**Corresponding Author:**
James G Patton
Department of Biological Sciences, Vanderbilt University
james.g.patton@vanderbilt.edu

Keywords: miRNA, miR-100, miR-125b, Colorectal Cancer, Cingulin, Invasiveness, Tight Junctions

Number of words in main text: 4,578
Number of figures/tables in main text: 7

Abstract

Extracellular communication via the transfer of vesicles and nanoparticles is now recognized to play an important role in tumor microenvironment interactions. Colorectal cancer (CRC) cells upregulate and secrete abundant levels of *miR-100* and *miR-125b* that can alter gene expression by cell- and non-cell-autonomous mechanisms. We previously showed that these miRNAs activate Wnt signaling through noncanonical pairing with 5 negative regulators of Wnt signaling. To identify additional targets of *miR-100* and *miR-125b*, we used bioinformatic approaches comparing multiple CRC cell lines, including knockout lines lacking one or both miRNAs. From an initial list of 96 potential mRNA targets, we tested 15 targets with 8 showing significant downregulation in the presence of *miR-100* and *miR-125b*. Among these, Cingulin (CGN) and Protein tyrosine phosphatase receptor type-R (PTPRR) are downregulated in multiple cancers, consistent with regulation by increased levels of *miR-100* and *miR-125b.* We also show that increased levels of *miR-100* and *miR-125b* enhance 3D growth and invasiveness. Lastly, we show that *miR-100* and *miR-125b* can be functionally transferred between cells to silence both reporter and endogenous mRNA targets.

1 Introduction

MicroRNAs (miRNAs) are small (22-23nt) RNAs that base pair with target mRNAs to regulate gene expression by decreasing translation and promoting RNA degradation (He and Hannon, 2004, Krol et al., 2010). In cancer, miRNA expression patterns are frequently altered, contributing to all aspects of tumor progression from proliferation to metastasis (Peng and Croce, 2016). We and others have focused on the role of *miR-100* and *miR-125b* in cancer (Cha et al., 2015, Qin et al., 2015, Peng et al., 2021, Liu et al., 2022, Lu et al., 2017, Zhang et al., 2021). These miRNAs are encoded in the third intron of *MIR100HG*, a 3kb lncRNA that is transcribed from the large 330kb MIR100HG locus (Emmrich et al., 2014). Increased expression of *miR-100, miR-125* and *MIR100HG* can promote cetuximab (anti-EGFR) resistance in colorectal cancer (CRC) cells, drive progression of pancreatic cancer, and promote the epithelial to mesenchymal transition (Lu et al., 2017, Liu et al., 2022, Ottaviani et al., 2018). These effects are driven in part by regulating the expression of target mRNAs including mTOR (Cha et al., 2015), negative regulators of Wnt signaling (Lu et al., 2017), Cystic Fibrosis Transmembrane Regulator (CFTR) (Zhang et al., 2021), Cingulin (CGN) (Zhang et al., 2021), and checkpoint kinases (CHK) (Ottaviani et al., 2018). These are just a small subset of targets for these miRNAs; TargetScan predicts a large number of potential targets for *miR-100* (59 targets) and *miR-125b* (931 targets)(https://www.targetscan.org/vert_80/). Base pairing between miRNAs and target 3'-UTRs is typically imperfect, with canonical targets displaying extensive pairing between nucleotides 2-8 of the miRNA (the "seed" sequence) and variable complementarity throughout the rest of the miRNA (Bartel, 2009). However, even within the seed sequence, the extent of base pairing between miRNAs and their mRNA targets is highly variable making prediction of mRNA targets a challenge (Li et al., 2008, Riolo et al., 2021). Indeed, all 5 of the negative regulators of Wnt (DKK1, DKK3, ZNRF3, RNF43, and APC2) that we previously found to be targeted by *miR-100* and *miR-125b* are noncanonical targets, raising the question as to whether additional targets might contribute to cetuximab resistance and altered 3D growth.

Extracellular vesicles (EVs) and nanoparticles participate in cell-cell communication through the transfer of RNA, protein and lipids (Couch et al., 2021, Dixson et al., 2023). Among RNA cargo for EVs, transfer of miRNA is the most well characterized due to their small size and

the ability to experimentally monitor silencing of target mRNAs in recipient cells (O'Brien et al., 2020). We previously showed that *miR-100* and *miR-125b* are enriched in small EVs (sEVs) from CRC cells with Transwell co-culture experiments supporting extracellular transfer of these miRNAs to recipient cells (Cha et al., 2015). However, since the recipient cells in those transfer experiments expressed endogenous *miR-100* and *miR-125b*, it remains a possibility that the silencing of mRNA targets in recipient cells could be due to unexpected activation of the endogenous genes (Gruner and McManus, 2021).

To identify targets of *miR-100* and *miR-125b* and to definitively demonstrate extracellular transfer, we created cell lines with CRISPR/Cas9-mediated knockouts of *miR-100, miR-125b,* or both. Through extensive bioinformatic analyses of RNAseq data, we identified and tested 15 candidate targets for *miR-100* and *miR-125b* with the two most statistically significant being Cingulin (CGN) and Protein Tyrosine Phosphatase Receptor Type-R (PTPRR). We also show that *miR-100* and *miR-125b* contribute to enhanced 3D growth and invasiveness of CRC cells. Lastly, we demonstrate functional transfer of *miR-100* and *miR-125b* from donor to recipient cells leading to silencing of both reporter and endogenous mRNAs.

2 Materials and Methods

2.1 Cell Culture

CC and CC-CR CRC cells were obtained from the Coffey lab (Lu et al., 2017). All cell lines were confirmed to be free of mycoplasma contamination (Venor™GeM Mycoplasma Detection Kit, PCR-based, Sigma Aldrich Cat #MP0025). Cells were grown in Dulbecco's Modified Eagle's Medium (DMEM, Corning) supplemented with 10% fetal bovine serum (FBS, Corning), 1% L-glutamine (200 nM, Gibco), 1% MEM nonessential amino acids (Sigma Aldrich), and 1% penicillin-streptomycin (10,000 U/mL, Gibco) in 5% CO_2 at 37°C. Cells were passaged a maximum of 8 times before discarding.

2.2 Generation of Knockout Cell Lines

We used CRISPR/Cas9 multiplex genome engineering (Kabadi et al., 2014) to delete *miR100, miR125b,* or both. Guide RNAS (gRNAs) flanking the targeted locus were designed using the Benchling CRISPR gRNA Design Tool (https://www.benchling.com/crispr). Oligonucleotides containing gRNA sequences were first cloned into sgRNA expression vectors (Addgene #53186-53189) and then multiple gRNA cassettes were cloned into lentiviral expression vectors (pLV hUbC-Cas9-T2A-GFP; Addgene, #53190) using Golden Gate cloning technology. Lentiviral stocks were prepared in 293T cells and used to transduce CC-CR cells. Single GFP^+ cells were sorted into 96 cell plates and expanded. PCR amplification of genomic DNA from clonal GFP^+ cells was performed using primers flanking the gRNA target sequences to identify deletion clones.

2.3 Extracellular Vesicle Isolation

Cells were plated at 9.0×10^6 cells in T-175 flasks (Corning), with each EV collection using at least 3 flasks. Cells were grown to 80% confluency and washed 3 times with 1X PBS before media were replaced with DMEM lacking FBS and grown for 48 hours. Culture media were then collected and adherent cells were trypsinized and counted. Conditioned media were then centrifuged at increasing speeds and time: 1,000xg for 10 minutes (room temperature), 2,000xg for 20 minutes (4°C), and 10,000xg for 30 minutes (4°C). Crude EV pellets were

123 obtained after the conditioned media was centrifuged for 17 hours at 100,000xg (4°C). EV
124 pellets were then washed two times by resuspension in 1mL of 1X DPBS (Corning) and
125 centrifugation at 100,000xg for 70 minutes. Final pellets were resuspended in 100µl 1X DPBS.
126 Under these conditions, the EV pellets consist of a heterogenous mixture of sEVs with some
127 non-vesicular material (Jeppesen et al., 2019). This protocol was used to directly compare with
128 earlier results examining export of *miR-100 and miR-125b* into CRC EVs (Cha et al., 2015).
129 sEVs were quantified by protein concentration (Pierce BCA Protein Assay) and by Nanoparticle
130 Tracking Analysis (NTA, ZetaView Nanoparticle Tracking Analysis Instrument).

131 **2.4 qRT-PCR**

132 Total RNA from both whole cell and sEVs was isolated using TRIzol (Life
133 Technologies). Taqman small RNA assays (Life Technologies) were used to quantify miRNA
134 levels. A total of 10ng of RNA were utilized for each RT reaction; 0.67 µl of cDNA was used in
135 each 10µl qPCR reactions. qPCR was completed in either 96-well or 384-well plates using
136 Biorad CFX96 or CFX384 instruments. Fold changes were calculated as previously described
137 (Cha et al., 2015).

138 **2.5 Transfer Assays**

139 For Transwell co-culture assays, cells were plated in Transwell dishes with 0.4mm filters
140 (Corning, 3460) with 50,000 cells in the donor well and 300,000 cells in the recipient well.
141 Transwell co-cultures were grown for five days, changing media every 72 hours. Cells were
142 washed 3 times with 2 mL of 1X PBS; RNA was then collected from either donor or recipient
143 cells.

144 **2.6 AGO2 Immunoprecipitation**

145 For immunoprecipitation, anti-AGO2 (clone 11A9 antibody; MABE253, Sigma-Aldrich)
146 or control IgG antibodies were used. Ten 150cm dishes of either CC or CC-CR cells were grown
147 to 95% confluency. Cells were then scraped in ice cold PBS and centrifuged to collect cell
148 pellets in ice cold lysis buffer (20mM Tris HCl pH 7.5, 150 mM KCl, 0.5% NP40, 2mM EDTA,
149 1mM NaF, 0.5mM DTT). After centrifugation of insoluble cell debris, cell lysates were
150 incubated with Dynabeads. Prior to cell lysis, Dynabeads™ Protein G (ThermoFisher, 10003D)
151 were conjugated with antibodies by incubating overnight with rotation at 4°C and washed two
152 times with ice cold lysis buffer. Cell lysates were then added to the conjugated beads and
153 incubated at 4°C for six hours. Beads were gently washed with fresh lysis buffer and proteins
154 were eluted. For RNA isolation, beads were incubated with DNase and Proteinase K for 10
155 minutes at room temperature. Trizol was then added and incubated at room temp for 10 minutes
156 and RNA was isolated.

157 **2.7 Small RNA Sequencing**

158 RNA libraries were generated using the NEXTFlex Small RNA Library Preparation Kits
159 v3 (Perkin) with the following modifications: (1) 3′- and 5′-adaptors were diluted 1:8, (2) 3′-
160 adaptor ligations were performed overnight in multiple steps –25°C for 2 h, 20°C for 4 h and
161 16°C overnight, (3) following cDNA synthesis and before barcoding PCR, step F protocol was
162 followed, and (4) PCR amplification was 20 cycles. Following PCR amplification, individual
163 libraries were size-selected (136–200 bp product) using Pippin Prep (Sage Sciences). Size-
164 selected libraries were quantified using a Qubit Fluorometer. Libraries were checked for quality
165 and sequenced using Illumina short-read technology. Libraries were pooled and paired-end

166 sequencing (PE-150) of the pool (equimolar multiplexed libraries) was performed on the
167 NovaSeq6000 platform by the VANTAGE core (Vanderbilt University). Demultiplexing and
168 bioinformatic analyses were performed using the TIGER pipeline (Allen et al., 2018). Briefly,
169 Cutadapt (v1.16) was used to trim 3′ adaptors and all reads with <16 nucleotides (nts) were
170 removed (Martin, 2011). Quality control on both raw reads and adaptor-trimmed reads was
171 performed using FastQC (v0.11.9)(www.bioinformatics.babraham.ac.uk/projects/fastqc). The
172 adaptor-trimmed reads were mapped to the hg19 genome, with additional rRNA and tRNA
173 reference sequences using Bowtie1 (v1.1.2), allowing only one mismatch (Langmead and
174 Salzberg, 2012).

175 **2.8 Total RNA Sequencing**

176 Bulk RNA sequencing libraries were prepared using Universal RNAseq kits (Tecan).
177 Libraries were cleaned (Zymo), checked for quality using the Agilent bioanalyzer, quantified
178 (Qubit), and pooled based on equimolar concentrations. Pooled libraries were sequenced using
179 Illumina short-read technology based on PE150 on the NovaSeq6000 (Illumina). After
180 sequencing, samples (libraries) were demultiplexed and analyzed. Briefly, adapter sequences
181 were removed using Cutadapt v2.10)(Martin, 2011). Quality control of both raw reads and
182 adaptor-trimmed reads was performed using FastQC (v0.11.9). After adaptor trimming, reads
183 were aligned to the Gencode GRCh38.p13 genome using STAR (v2.7.8a)(Dobin et al., 2013).
184 FeatureCounts (v2.0.2)(Liao et al., 2014) was used to count the number of reads mapped to each
185 gene. Heatmap3 (Zhao et al., 2014) was used for cluster analysis and visualization. Differential
186 expression was analyzed by DESeq2 (v1.30.1)(Love et al., 2014). Significant differentially
187 expressed genes were determined with fold change >2 or <0.5, and adjusted p value (padj) <0.05.
188 Genome Ontology and KEGG pathway over-representation analyses were performed using the
189 WebGestaltR package (NULL)(Wang et al., 2017). Gene set enrichment analysis (GSEA) was
190 performed using GSEA package (v4.3.2)(Subramanian et al., 2005) on database v2022.1.Hs.

191 **2.9 Gene Expression Analysis**

192 The Gene Expression database of Normal and Tumor Tissues (GENT2) was used to
193 compare levels of expression between 72 paired normal and tumor tissues utilizing the GPL570
194 platform. Statistical significance was determined using two-sample t-tests (GPL570 platform
195 (HG-U133_Plus_2)).

196 **2.10 Luciferase Reporter Assays**

197 3'-UTRs from mRNAs of interests were cloned using RT/PCR into the pMIR-REPORT™
198 miRNA Expression Reporter Vector System (Firefly Luciferase) using NEBuilder HiFi DNA
199 Assembly (New England BioLabs). PCR amplification primers are listed in **Table S1**. All
200 plasmids were verified by sequencing (Genewiz). Transfected cells were cultured alone or in co-
201 cultures using Transwells with 0.4mm membranes for 72 hours followed by washing with 1X
202 PBS. Luciferase levels were then detected using the Dual-Glo® Luciferase Assay System
203 (Promega). Changes in luciferase levels were normalized to Renilla luciferase levels and
204 compared to luminescence from the empty (no 3'UTR) vector.

205 **2.11 Transfections**

206 Cells were grown to approximately 50-60% confluency with transfections performed
207 using TransIT®-2020 (Mirus, MIR5404). The Renilla luciferase construct (pClneo-RL, Plasmid
208 # 115366, Addgene) was transfected at 0.5ug/mL and firefly luciferase construct was transfected

209 at 1ug/mL. DNA and TransIT-2020 were incubated for 30 minutes at room temperature in
210 reduced serum media (Opti-MEM; Gibco). Transfection complexes were diluted 1:10 in DMEM
211 and added to cells.

212 **2.12 Immunofluorescence Staining and Imaging of Cells**

213 Cells were plated on coverslips and grown for three days after which coverslips were
214 washed three times in 1x PBS and fixed in 4% paraformaldehyde for 30 minutes at room
215 temperature. Samples were then washed and allowed to block for 1 hour at room temperature in
216 blocking buffer (1X PBS with 0.001% Triton-X and 0.03% donkey serum). Primary antibody
217 incubation (CGN, ab244406) was overnight at 4°C, followed by three 1X PBS wash steps, and
218 incubation with secondary antibodies (Cy3 anti-Rabbit antibody and 488 conjugated phalloidin)
219 for 2 hours at room temperature. Samples were washed three times with 1X PBS and mounted
220 on glass slides using Vectashield with DAPI and imaged using a Zeiss LSM 880 microscope
221 (Vanderbilt University, CISR). All images were analyzed using ImageJ (Aebi et al., 1986).

222 **2.13 Spheroid Cultures**

223 Cells (10,000) were plated in Nunclon Sphera low adherent plates (Thermo Scientific)
224 and centrifuged at 1,000xg for 10 minutes at room temperature, as previously described (Carey et
225 al., 2013). Cells were grown for three days before transfer into 2mg/ml Type I collagen
226 (Advanced Biomatrix). Colonies were imaged using Muvicyte Live Cell imager for five days.
227 Images were processed and analyzed using ImageJ(Aebi et al., 1986).

228 **3 Results**

229 To facilitate identification of mRNA targets for *miR-100* and *miR-125b* and to develop
230 cell lines to test for functional miRNA transfer, we used CRISPR/Cas9 technology to generate
231 deletions in the MIR100HG locus for these two miRNAs (**Fig. 1A**). A single lentiviral vector
232 expressing multiple gRNAs, Cas9, and GFP was created and lentiviruses were transduced into
233 CC-CR cells. CC-CR cells are cetuximab resistant cells that were generated from CC cells by
234 iterative cycles of selection under 2D (resistant) and 3D (sensitive) growth conditions (Lu et al.,
235 2017). The gRNAs were designed to base pair with regions flanking *miR-100, miR-125b,* or
236 both (**Fig. S1**). Individual GFP+ clones were sorted, targeted deletions were identified by PCR,
237 and verified by sequencing. While CC-CR cells express high levels of *miR-100* and *miR-125b*,
238 CC cells express ~50-fold less of both miRNAs (Lu et al., 2017), and our different knockout
239 lines showed undetectable levels of *miR-100 or miR-125b or both* **(Fig. 1B, C).**

240 **3.1 Identification of mRNA Targets of *miR-100 and miR125b***

241 RNAseq was performed on CC, CC-CR, and knockout cells (Δ*miR-100*, Δ*miR-125b*, and
242 Δ*miR-100/miR-125b*) and bioinformatic analyses were performed to compare gene expression
243 patterns (**Table S2**). Potential mRNA targets for *miR-100* and *miR-125b* were identified using a
244 three-step strategy (**Fig. 2A).** First, we identified upregulated mRNAs in both CC and Δ*miR-*
245 *100/miR-125b* cells compared to CC-CR cells (Lu et al., 2017). Second, we compiled a list of
246 predicted targets for *miR-100* and *miR-125b* using three different prediction algorithms
247 (TargetScan, TargetMiner, and miRDB; https://www.targetscan.org/vert_80/;
248 https://www.isical.ac.in/~bioinfo_miu/targetminer20.htm; https://mirdb.org/). Third, we
249 performed RNA immunoprecipitation of AGO2 followed by bulk and short RNA sequencing
250 (**Tables S3,4**). AGO2 is a component of the RNA Induced Silencing Complex (RISC) in which
251 miRNAs pair with their target mRNAs (Müller et al., 2020, Cenik and Zamore, 2011, Farazi et

252 al., 2008, Liu et al., 2004). Immunoprecipitation of AGO2-containing complexes from CC-CR
253 cells allowed for enrichment of *miR-100* and *miR-125b* targets because these miRNAs are so
254 highly expressed in CC-CR cells (Lu et al., 2017). By comparing the three sets of data, we were
255 able to identify overlapping targets of *miR-100* and *miR-125b* (**Fig. 2A**). Together, we identified
256 51 potential targets for *miR-100* and 45 potential targets for *miR-125b* (**Fig. 2B**). When we
257 subjected all 96 potential targets to Gene Ontology analysis using ShinyGo (Ge et al., 2020), we
258 found significant enrichment for cell migration, cell motility, actin filament-based processes, and
259 MAPK signaling (**Fig. 2C; Table S5**).

260 **3.2 Silencing of mRNA Targets of *miR-100* and *miR-125b***

261 From the targets generated above, we examined miRNA:mRNA pairing (**Fig. S2**) and
262 selected 15 candidate mRNAs to test for the ability of *miR-100* (3 candidates), *miR-125b* (7
263 candidates) or both (5 candidates) to silence luciferase reporter constructs. We designed three
264 different categories of luciferase vectors in which the firefly luciferase open reading frame was
265 fused to (1) no 3'-UTR (empty vector), (2) 3'-UTRs containing three perfect binding sites for
266 *miR-100* or *miR-125b* (100/125 vector), or (3) 3'-UTRs from candidate targets (experimental
267 vectors)(**Fig. 3A**). These vectors were transfected into either CC-CR or Δ*miR-100/miR-125b*
268 cells and luciferase levels were determined. *Bona fide* targets of *miR-100 or miR-125b* should
269 show increased luciferase levels in Δ*miR-100/miR-125b* cells as compared to CC-CR cells. Of
270 the 15 targets we tested, 14 showed increased luciferase levels in Δ*miR-100/miR-125b* cells with
271 8 being statistically significant (**Fig. 3B**). Of the 8, CGN and PTPRR showed the most
272 significant increase of luciferase activity when comparing Δ*miR-100/miR-125b* and CC-CR cells
273 (**Fig. 3B**). The fact that the two most significant genes are targets of *miR-125b* is consistent with
274 more dramatic overexpression of *miR-125b* in CC-CR cells as compared to *miR-100* (**Fig. 1B**).

275 **3.3 CGN and PTPRR are Downregulated in Colorectal Cancer**

276 *miR-100* and *miR-125b* display elevated gene expression and target multiple mRNAs in
277 CRC and other cancer types (Li et al., 2015, Wang et al., 2020, Ottaviani et al., 2018, Cha et al.,
278 2015, Lu et al., 2017, Zhang et al., 2021, Vallacchi and Rodolfo, 2018). Consistent with that,
279 CC-CR cells form solid, disorganized colonies when grown in collagen, indicative of aggressive
280 behavior, as opposed to CC cells which form hollow cysts with a central lumen lined by
281 polarized cells (Lu et al., 2017). We thus sought to test if decreased expression of CGN and
282 PTPRR due to increased expression of *miR-100* and *miR-125b* might be observed in CRC and
283 other cancers. We used the GENT2 database to compare the levels of CGN and PTPRR between
284 normal and cancer tissues (**Fig. 4A,B**). We found that CGN and PTPRR are both downregulated
285 across a variety of cancers, including CRC. There are likely additional mechanisms that can lead
286 to decreased levels of CGN and PTPRR because not all cancers show increased expression of
287 *miR-100* (Li et al., 2015) or *miR-125b* (Wang et al., 2020), but the data are in agreement that
288 decreased levels of CGN and PTPRR correlate with cancer.

289 **3.4 Extracellular Transfer of *miR-100* and *miR-125b***

290 Experiments proposing extracellular miRNA transfer can generate false positives if the
291 recipient cell lines express the same miRNAs being tested (Gruner and McManus, 2021). Our
292 knockout cell lines provide an ideal control to test for extracellular transfer of *miR-100* and *miR-*
293 *125b* because Δ*miR-100/miR-125b* cells do not express either miRNA. As donor cells, we used
294 CC-CR cells because they not only express high levels of *miR-100* and *miR-125b*, they also
295 secrete EVs enriched in both miRNAs (**Fig. 5A).** Thus, we set up Transwell assays with CC-CR

296 donor cells and Δ*miR-100/miR-125b* recipient cells and co-cultured the cells for 5 days before
297 isolation of RNA from the recipient cells. Compared to control transfer experiments in which
298 Δ*miR-100/miR-125b* cells were used as both the donor and recipient cells, we observed dramatic
299 increases in the levels of *miR-100* and *miR-125b* in Δ*miR-100/miR-125b* recipient cells (~150-
300 and 60-fold, respectively) when CC-CR cells were used as the donor (**Fig. 5B**).

301 To determine whether the transfer of *miR-100* and *miR-125b* from CC-CR cells to Δ*miR-*
302 *100/miR-125b* recipient cells results in functional miRNA transfer, we used Transwell co-culture
303 assays in which the Δ*miR-100/miR-125b* recipient cells were transfected with vectors in which
304 the firefly luciferase open reading frame was fused to the 3'-UTRs from either CGN or PTPRR
305 (**Fig. 5C**). Compared to controls, we observed a significant reduction in luciferase levels when
306 CC-CR cells were the donor cells and Δ*miR-100/miR-125b* were the recipient cells (**Fig. 5D**).
307 These data demonstrate that *miR-100 and miR-125b* can be functionally transferred between cells
308 to silence reporter mRNAs.

309 As an additional test of functional extracellular transfer of *miR-100 and miR-125b,* we
310 next tested whether we could observe silencing of the endogenous CGN gene in recipient cells
311 by immunofluorescence staining. Cingulin connects tight junctions to the cytoskeleton and
312 localizes to apical junctions joining adjacent epithelial cells (Zhang et al., 2021, Citi et al., 1988).
313 In cells that express low to undetectable levels of *miR-100 or miR-125b* (CC and Δ*miR-100/miR-*
314 *125b* cells), CGN was readily detected and localized to cell-cell junctions (**Fig. 6A**).
315 Immunofluorescent signals were more readily visualized in CC cells compared to Δ*miR-*
316 *100/miR-125b* cells, potentially due to regulation of other factors by *miR-100 or miR-125b* that
317 also seem to affect overall morphology, as indicated by differences in F-actin staining and
318 changes in CGN localization. Nevertheless, in cells expressing high levels of *miR-100* and *miR-*
319 *125b* (CC-CR cells), CGN detection was dramatically reduced, and at least partially reversed by
320 deletion of *miR-100* and *miR-125b* (**Fig. 6A**). These data support targeting of CGN by *miR-100*
321 and *miR-125b.*

322 With baseline levels of CGN immunofluorescence in hand, we next used Transwell co-
323 culture experiments with CC-CR donor cells and Δ*miR-100/miR-125b* recipient cells and
324 performed immunofluorescent staining of CGN in recipient cells. With Δ*miR-100/miR-125b*
325 donor cells, we were able to detect CGN in recipient cells (**Fig. 6B**) at levels similar to those
326 observed in **Fig. 6A**. However, when CC-CR cells were used as the donor cells, CGN was
327 undetectable in Δ*miR-100/miR-125b* recipient cells when measured by immunofluorescence
328 (**Fig. 6B**). These results provide strong evidence that CGN protein levels are downregulated by
329 functional transfer of *miR-100* and *miR-125b*.

330 **3.5 *miR-100* and *miR-125b* Contribute to Enhanced 3D Growth and Invasiveness**

331 Gene Ontology analysis of targets of miR-100 and miR-125b showed enrichment in
332 genes associated with cell migration and motility (**Fig. 2C**). This is consistent with
333 downregulation of CGN which leads to increased invasiveness, metastatic potential, and EMT
334 (Guillemot and Citi, 2006, Mangan et al., 2016, Schossleitner et al., 2016, Zhang et al., 2021).
335 To test the effect of *miR-100* and *miR-125b* and targeting of CGN on 3D growth, we cultured
336 CC, CC-CR and Δ*miR-100/miR-125b* cells under spheroid growth conditions (Carey et al., 2013)
337 in low adherence plates for 3 days before transfer to growth in Type I collagen. Under these

338 conditions at both day 0 and day 5 in collagen, the morphology of Δ*miR-100/miR-125b* colonies
339 was more similar to CC colonies than to colonies derived from parental CC-CR cells (**Fig. 7A**;
340 **Supp. Movies 1-3**). At day 5, we also observed significant differences in surface dynamics
341 when comparing colonies derived from the three lines **(Supp. Movies 1-3)**. Increased
342 projections emanating from the edges of the colonies and protruding into collagen were observed
343 with CC-CR cells, whereas far fewer projections were observed in colonies derived from CC
344 cells grown under the same conditions. As with overall morphology, Δ*miR-100/miR-125b*
345 colony dynamics and projections were more similar to that observed in CC colonies than CC-CR
346 colonies **(Supp. Movies 1-3).**

347 Quantification of overall spheroid growth revealed that colonies derived from CC-CR
348 cells showed a significant increase in total spheroid area when compared to colonies derived
349 from CC or Δ*miR-100/miR-125b* cells (**Fig. 7B**). We also quantified the number and size of
350 projections into the collagen as a measure of invasiveness by determining the increase in
351 projection surface area after growth in collagen for five days. CC-CR colonies showed a
352 significantly greater increase in projection area compared to CC and Δ*miR-100/miR-125b*
353 colonies (**Fig. 7C**). While invasiveness is likely due to multiple changes, the decreased
354 projections we observe in CC and Δ*miR-100/miR-125b* colonies are consistent with increased
355 expression of CGN due to lower levels of *miR-100* and *miR-125b*.

356 **4 Discussion**

357 Several reports have supported the hypothesis that miRNAs can transfer from one cell to
358 another via extracellular mechanisms (Mittelbrunn et al., 2011, Valadi et al., 2007, Skog et al.,
359 2008, Boelens et al., 2014, Squadrito et al., 2014, Cha et al., 2015, Barman et al., 2022). While
360 these reports show that miRNA can be transferred between cells, the recipient cells often express
361 the same miRNAs, potentially complicating interpretation of target mRNA silencing in recipient
362 cells (Gruner and McManus, 2021). Silencing under these conditions could be due to an
363 unexpected increased expression of endogenous miRNAs as opposed to functional miRNA
364 transfer. Our knockout cell lines provide an ideal control to obviate such concerns and
365 demonstrate functional miRNA transfer. Using donor cells that express high levels of *miR-100*
366 and *miR-125b* and recipient cells with targeted deletions of these genes, we identified mRNA
367 targets and demonstrated functional transfer of *miR-100* and *miR-125b* between cells to silence
368 both reporter constructs and endogenous mRNA transcripts in recipient cells. Decreased
369 expression of CGN in recipient cells is especially important because it validates silencing
370 without the use of reporter constructs.

371 **4.1 Tumor Microenvironment Implications**

372 Invasiveness and metastasis are indicative of differing stages of colorectal cancer and can
373 also be indicative of patient prognosis (Hanahan and Weinberg, 2011, Zeineddine et al., 2023).
374 EMT is a pivotal stage of metastasis involving the breakdown of cell-cell adhesions (Pretzsch et
375 al., 2019). Located on apical regions of adjacent epithelial cells, tight junctions play a crucial
376 role in cell-cell adhesion and tissue integrity. Disruption of tight junctions can allow cells to
377 become invasive and metastatic (Martin, 2014). CGN serves as a tether between the
378 cytoskeleton and tight junction components, interacting with ZO-1 at apical junctions (Zihni et
379 al., 2016, Citi et al., 1988). Loss of CGN in epithelial cells has been shown to disrupt tight
380 junction formation and cell polarity (Mangan et al., 2016, Guillemot and Citi, 2006,
381 Schossleitner et al., 2016). Coupled to our finding that *miR-100* and *miR-125b* are enriched in

382 EVs from CRC cells and that *miR-100* and *miR-125b* can be transferred between cells, our data
383 support a model whereby cell-cell communication within the tumor microenvironment can alter
384 tight junctions leading to altered growth and increased metastatic potential in recipient cells. For
385 PTPRR, transfer of *miR-100* and *miR-125b* leading to decreased levels of PTPRR would be
386 expected to activate Wnt signaling since it is a negative regulator of the Wnt pathway (Wang et
387 al., 2019). This is consistent with activation of Wnt signaling in aggressive CC-CR cells (Lu et
388 al., 2017).

389 **4.2 Tumor Growth and Invasiveness**

390 Beyond demonstrating miRNA transfer between cells, our knockout lines provided a
391 model to test the effects of 3D growth in the presence and absence of *miR-100* and *miR-125b.* In
392 3D growth in collagen, CC cells form hollow cysts with a central lumen lined by polarized cells
393 whereas CC-CR cells grow into the central lumen with disorganized, solid colonies (Lu et al.,
394 2017). A prior deletion of exon 4 within the MIR100HG locus supported the idea that
395 MIR100HG contributes to both cetuximab resistance and metastasis (Liu et al., 2022). Our
396 precise deletions of *miR-100* and *miR-125b* allowed us to test the effect of these miRNAs on 3D
397 growth and showed that loss of these miRNAs results in slower overall growth with decreased
398 edge dynamics and fewer invasive projections. Since expression of MIR100HG is unaffected in
399 our knockout lines, our data agree with previous results that *MIR100HG* can induce EMT, but
400 also that *miR-100* and *miR-125b* play a similar role through downregulation of CGN (Zhang et
401 al., 2021). The data are also consistent with our GO analysis of the targets of *miR-100* and *miR-*
402 *125b* being enriched in cell motility and migration (**Fig 2C**).

403 In summary, our data support findings that increased expression of *miR-100* and *miR-*
404 *125b* in cancer promotes disruption of tight junctions, activation of EMT, and increased
405 metastatic potential. Given that these miRNAs are abundant in EVs secreted from CRC cells,
406 the data support both cell-autonomous and non cell-autonomous roles for *miR-100* and *miR-*
407 *125b.*

408 **5 Acknowledgements**

409 The authors would like to thank all members of the Coffey, Weaver, and Patton labs for
410 advice and suggestions.

411 **6 Funding**

412 This work was supported by PO1 CA229123 to RJC, AMW, KCV, QL, and JGP.

413 **7 Author Contributions**

414 HMN, SQ, SC, NL, SS, LT, MS, LG, and KCC generated all data in the manuscript. KCV, QL,
415 JLF, AMW, MR, and RJC provided scientific advice and suggestions and edited the manuscript.
416 HMN, SQ, JLF, MR and JGP wrote the paper.

417 **8 References**

418 AEBI, M., HORNIG, H., PADGETT, R. A., REISER, J. & WEISSMAN, C. 1986. Sequence requirements
419 for splicing of higher eukaryotic nuclear pre-mRNA. *Cell,* 47**,** 555-565.
420 ALLEN, R. M., ZHAO, S., RAMIREZ SOLANO, M. A., ZHU, W., MICHELL, D. L., WANG, Y., SHYR, Y.,
421 SETHUPATHY, P., LINTON, M. F., GRAF, G. A., SHENG, Q. & VICKERS, K. C. 2018.
422 Bioinformatic analysis of endogenous and exogenous small RNAs on lipoproteins. *J*
423 *Extracell Vesicles,* 7**,** 1506198.
424 BARMAN, B., SUNG, B. H., KRYSTOFIAK, E., PING, J., RAMIREZ, M., MILLIS, B., ALLEN, R., PRASAD,
425 N., CHETYRKIN, S., CALCUTT, M. W., VICKERS, K., PATTON, J. G., LIU, Q. & WEAVER, A. M.
426 2022. VAP-A and its binding partner CERT drive biogenesis of RNA-containing
427 extracellular vesicles at ER membrane contact sites. *Dev Cell,* 57**,** 974-994 e8.
428 BARTEL, D. P. 2009. MicroRNAs: target recognition and regulatory functions. *Cell,* 136**,** 215-33.
429 BOELENS, M. C., WU, T. J., NABET, B. Y., XU, B., QIU, Y., YOON, T., AZZAM, D. J., TWYMAN-SAINT
430 VICTOR, C., WIEMANN, B. Z., ISHWARAN, H., TER BRUGGE, P. J., JONKERS, J.,
431 SLINGERLAND, J. & MINN, A. J. 2014. Exosome transfer from stromal to breast cancer
432 cells regulates therapy resistance pathways. *Cell,* 159**,** 499-513.
433 CAREY, S. P., STARCHENKO, A., MCGREGOR, A. L. & REINHART-KING, C. A. 2013. Leading
434 malignant cells initiate collective epithelial cell invasion in a three-dimensional
435 heterotypic tumor spheroid model. *Clin Exp Metastasis,* 30**,** 615-30.
436 CENIK, E. S. & ZAMORE, P. D. 2011. Argonaute proteins. *Curr Biol,* 21**,** R446-9.
437 CHA, D. J., FRANKLIN, J. L., DOU, Y., LIU, Q., HIGGINBOTHAM, J. N., BECKLER, M. D., WEAVER, A.
438 M., VICKERS, K., PRASAD, N., LEVY, S., ZHANG, B., COFFEY, R. J. & PATTON, J. G. 2015.
439 KRAS-dependent sorting of miRNA to exosomes. *eLife,* 4**,** e07197.
440 CITI, S., SABANAY, H., JAKES, R., GEIGER, B. & KENDRICK-JONES, J. 1988. Cingulin, a new
441 peripheral component of tight junctions. *Nature,* 333**,** 272-276.
442 COUCH, Y., BUZAS, E. I., DI VIZIO, D., GHO, Y. S., HARRISON, P., HILL, A. F., LOTVALL, J., RAPOSO,
443 G., STAHL, P. D., THERY, C., WITWER, K. W. & CARTER, D. R. F. 2021. A brief history of
444 nearly EV-erything - The rise and rise of extracellular vesicles. *J Extracell Vesicles,* 10**,**
445 e12144.
446 DIXSON, A. C., DAWSON, T. R., DI VIZIO, D. & WEAVER, A. M. 2023. Context-specific regulation
447 of extracellular vesicle biogenesis and cargo selection. *Nat Rev Mol Cell Biol*.
448 DOBIN, A., DAVIS, C. A., SCHLESINGER, F., DRENKOW, J., ZALESKI, C., JHA, S., BATUT, P.,
449 CHAISSON, M. & GINGERAS, T. R. 2013. STAR: ultrafast universal RNA-seq aligner.
450 *Bioinformatics,* 29**,** 15-21.
451 EMMRICH, S., STRELTSOV, A., SCHMIDT, F., THANGAPANDI, V. R., REINHARDT, D. & KLUSMANN,
452 J. H. 2014. LincRNAs MONC and MIR100HG act as oncogenes in acute megakaryoblastic
453 leukemia. *Mol Cancer,* 13**,** 171.
454 FARAZI, T. A., JURANEK, S. A. & TUSCHL, T. 2008. The growing catalog of small RNAs and their
455 association with distinct Argonaute/Piwi family members. *Development,* 135**,** 1201-14.
456 GE, S. X., JUNG, D. & YAO, R. 2020. ShinyGO: a graphical gene-set enrichment tool for animals
457 and plants. *Bioinformatics,* 36**,** 2628-2629.
458 GRUNER, H. N. & MCMANUS, M. T. 2021. Examining the evidence for extracellular RNA function
459 in mammals. *Nat Rev Genet,* 22**,** 448-458.

460 GUILLEMOT, L. & CITI, S. 2006. Cingulin regulates claudin-2 expression and cell proliferation
461 through the small GTPase RhoA. *Mol Biol Cell,* 17**,** 3569-77.
462 HANAHAN, D. & WEINBERG, R. A. 2011. Hallmarks of cancer: the next generation. *Cell,* 144**,**
463 646-74.
464 HE, L. & HANNON, G. J. 2004. MicroRNAs: small RNAs with a big role in gene regulation. *Nat Rev*
465 *Genet,* 5**,** 522-31.
466 JEPPESEN, D. K., FENIX, A. M., FRANKLIN, J. L., HIGGINBOTHAM, J. N., ZHANG, Q., ZIMMERMAN,
467 L. J., LIEBLER, D. C., PING, J., LIU, Q., EVANS, R., FISSELL, W. H., PATTON, J. G., ROME, L.
468 H., BURNETTE, D. T. & COFFEY, R. J. 2019. Reassessment of Exosome Composition. *Cell,*
469 177**,** 428-445 e18.
470 KABADI, A. M., OUSTEROUT, D. G., HILTON, I. B. & GERSBACH, C. A. 2014. Multiplex
471 CRISPR/Cas9-based genome engineering from a single lentiviral vector. *Nucleic Acids*
472 *Res,* 42**,** e147.
473 KROL, J., LOEDIGE, I. & FILIPOWICZ, W. 2010. The widespread regulation of microRNA
474 biogenesis, function and decay. *Nat Rev Genet,* 11**,** 597-610.
475 LANGMEAD, B. & SALZBERG, S. L. 2012. Fast gapped-read alignment with Bowtie 2. *Nat*
476 *Methods,* 9**,** 357-9.
477 LI, C., GAO, Y., ZHANG, K., CHEN, J., HAN, S., FENG, B., WANG, R. & CHEN, L. 2015. Multiple
478 Roles of MicroRNA-100 in Human Cancer and its Therapeutic Potential. *Cell Physiol*
479 *Biochem,* 37**,** 2143-59.
480 LI, N., FLYNT, A., KIM, H. R., SOLNICA-KREZEL, L. & PATTON, J. 2008. Dispatched Homolog 2 is
481 targeted by miR-214 through a combination of three weak microRNA recognition sites.
482 *Nucleic Acids Res,* 36**,** 4277-85.
483 LIAO, Y., SMYTH, G. K. & SHI, W. 2014. featureCounts: an efficient general purpose program for
484 assigning sequence reads to genomic features. *Bioinformatics,* 30**,** 923-30.
485 LIU, H., LI, D., SUN, L., QIN, H., FAN, A., MENG, L., GRAVES-DEAL, R., GLASS, S. E., FRANKLIN, J. L.,
486 LIU, Q., WANG, J., YEATMAN, T. J., GUO, H., ZONG, H., JIN, S., CHEN, Z., DENG, T., FANG,
487 Y., LI, C., KARIJOLICH, J., PATTON, J. G., WANG, X., NIE, Y., FAN, D., COFFEY, R. J., ZHAO,
488 X. & LU, Y. 2022. Interaction of lncRNA MIR100HG with hnRNPA2B1 facilitates m(6)A-
489 dependent stabilization of TCF7L2 mRNA and colorectal cancer progression. *Mol Cancer,*
490 21**,** 74.
491 LIU, J., CARMELL, M. A., RIVAS, F. V., MARSDEN, C. G., THOMSON, J. M., SONG, J. J., HAMMOND,
492 S. M., JOSHUA-TOR, L. & HANNON, G. J. 2004. Argonaute2 is the catalytic engine of
493 mammalian RNAi. *Science,* 305**,** 1437-41.
494 LOVE, M. I., HUBER, W. & ANDERS, S. 2014. Moderated estimation of fold change and
495 dispersion for RNA-seq data with DESeq2. *Genome Biol,* 15**,** 550.
496 LU, Y., ZHAO, X., LIU, Q., LI, C., GRAVES-DEAL, R., CAO, Z., SINGH, B., FRANKLIN, J. L., WANG, J.,
497 HU, H., YANG, M., YEATMAN, T. J., LEE, E., SAITO-DIAZ, K., HINGER, S., PATTON, J. G.,
498 CHUNG, C. H., EMMRICH, S., KLUSMANN, J.-H., FAN, D. & COFFEY, R. J. 2017. lncRNA
499 MIR100HG-derived miR-100 and miR-125b mediate Cetuximab resistance via Wnt/beta
500 catenin signaling. *Nature Medicine,* 23**,** 1331-1341.
501 MANGAN, A. J., SIETSEMA, D. V., LI, D., MOORE, J. K., CITI, S. & PREKERIS, R. 2016. Cingulin and
502 actin mediate midbody-dependent apical lumen formation during polarization of
503 epithelial cells. *Nat Commun,* 7**,** 12426.

504 MARTIN, M. 2011. Cutadapt removes adapator sequences from high-throughput sequencing
505 reads. *EMBnet.journal,* 17**,** 10-12.
506 MARTIN, T. A. 2014. The role of tight junctions in cancer metastasis. *Semin Cell Dev Biol,* 36**,**
507 224-31.
508 MITTELBRUNN, M., GUTIERREZ-VAZQUEZ, C., VILLARROYA-BELTRI, C., GONZALEZ, S., SANCHEZ-
509 CABO, F., GONZALEZ, M. A., BERNAD, A. & SANCHEZ-MADRID, F. 2011. Unidirectional
510 transfer of microRNA-loaded exosomes from T cells to antigen-presenting cells. *Nat*
511 *Commun,* 2**,** 282.
512 MÜLLER, M., FAZI, F. & CIAUDO, C. 2020. Argonaute Proteins: From Structure to Function in
513 Development and Pathological Cell Fate Determination. *Frontiers in Cell and*
514 *Developmental Biology,* 7.
515 O'BRIEN, K., BREYNE, K., UGHETTO, S., LAURENT, L. C. & BREAKEFIELD, X. O. 2020. RNA delivery
516 by extracellular vesicles in mammalian cells and its applications. *Nat Rev Mol Cell Biol,*
517 21**,** 585-606.
518 OTTAVIANI, S., STEBBING, J., FRAMPTON, A. E., ZAGORAC, S., KRELL, J., DE GIORGIO, A.,
519 TRABULO, S. M., NGUYEN, V. T. M., MAGNANI, L., FENG, H., GIOVANNETTI, E., FUNEL,
520 N., GRESS, T. M., JIAO, L. R., LOMBARDO, Y., LEMOINE, N. R., HEESCHEN, C. &
521 CASTELLANO, L. 2018. TGF-beta induces miR-100 and miR-125b but blocks let-7a
522 through LIN28B controlling PDAC progression. *Nat Commun,* 9**,** 1845.
523 PENG, B., THENG, P. Y. & LE, M. T. N. 2021. Essential functions of miR-125b in cancer. *Cell Prolif,*
524 54**,** e12913.
525 PENG, Y. & CROCE, C. M. 2016. The role of MicroRNAs in human cancer. *Signal Transduction*
526 *and Targeted Therapy,* 1**,** 15004.
527 PRETZSCH, E., BÖSCH, F., NEUMANN, J., GANSCHOW, P., BAZHIN, A., GUBA, M., WERNER, J. &
528 ANGELE, M. 2019. Mechanisms of Metastasis in Colorectal Cancer and Metastatic
529 Organotropism: Hematogenous versus Peritoneal Spread. *J Oncol,* 2019**,** 7407190.
530 QIN, C., HUANG, R. Y. & WANG, Z. X. 2015. Potential role of miR-100 in cancer diagnosis,
531 prognosis, and therapy. *Tumour Biol,* 36**,** 1403-9.
532 RIOLO, G., CANTARA, S., MARZOCCHI, C. & RICCI, C. 2021. miRNA Targets: From Prediction Tools
533 to Experimental Validation. *Methods and Protocols,* 4.
534 SCHOSSLEITNER, K., RAUSCHER, S., GROGER, M., FRIEDL, H. P., FINSTERWALDER, R.,
535 HABERTHEUER, A., SIBILIA, M., BROSTJAN, C., FODINGER, D., CITI, S. & PETZELBAUER, P.
536 2016. Evidence That Cingulin Regulates Endothelial Barrier Function In Vitro and In Vivo.
537 *Arterioscler Thromb Vasc Biol,* 36**,** 647-54.
538 SKOG, J., WÜRDINGER, T., RIJN, S. V., MEIJER, D. H., GAINCHE, L., JR, W. T. C., CARTER, B. S.,
539 KRICHEVSKY, A. M. & BREAKEFIELD, X. O. 2008. Glioblastoma microvesicles transport
540 RNA and proteins that promote tumour growth and provide diagnostic biomarkers.
541 *Nature Cell Biology,* 10**,** 1470.
542 SQUADRITO, M. L., BAER, C., BURDET, F., MADERNA, C., GILFILLAN, G. D., LYLE, R., IBBERSON,
543 M. & DE PALMA, M. 2014. Endogenous RNAs Modulate MicroRNA Sorting to Exosomes
544 and Transfer to Acceptor Cells. *Cell Rep,* 8**,** 1432-46.
545 SUBRAMANIAN, A., TAMAYO, P., MOOTHA, V. K., MUKHERJEE, S., EBERT, B. L., GILLETTE, M. A.,
546 PAULOVICH, A., POMEROY, S. L., GOLUB, T. R., LANDER, E. S. & MESIROV, J. P. 2005.

547 Gene set enrichment analysis: a knowledge-based approach for interpreting genome-
548 wide expression profiles. *Proc Natl Acad Sci U S A,* 102**,** 15545-50.
549 VALADI, H., EKSTROM, K., BOSSIOS, A., SJOSTRAND, M., LEE, J. J. & LOTVALL, J. O. 2007.
550 Exosome-mediated transfer of mRNAs and microRNAs is a novel mechanism of genetic
551 exchange between cells. *Nat Cell Biol,* 9**,** 654-9.
552 VALLACCHI, V. & RODOLFO, M. 2018. miR-100 and miR-125b regulate epithelial-mesenchymal
553 transition and drug resistance in tumors. *Non-coding RNA Investigation,* 2**,** 57-61.
554 WANG, J., VASAIKAR, S., SHI, Z., GREER, M. & ZHANG, B. 2017. WebGestalt 2017: a more
555 comprehensive, powerful, flexible and interactive gene set enrichment analysis toolkit.
556 *Nucleic Acids Res,* 45**,** W130-W137.
557 WANG, Y., CAO, J., LIU, W., ZHANG, J., WANG, Z., ZHANG, Y., HOU, L., CHEN, S., HAO, P., ZHANG,
558 L., ZHUANG, M., YU, Y., LI, D. & FAN, G. 2019. Protein tyrosine phosphatase receptor
559 type R (PTPRR) antagonizes the Wnt signaling pathway in ovarian cancer by
560 dephosphorylating and inactivating beta-catenin. *J Biol Chem,* 294**,** 18306-18323.
561 WANG, Y., ZENG, G. & JIANG, Y. 2020. The Emerging Roles of miR-125b in Cancers. *Cancer*
562 *Manag Res,* 12**,** 1079-1088.
563 ZEINEDDINE, F. A., ZEINEDDINE, M. A., YOUSEF, A., GU, Y., CHOWDHURY, S., DASARI, A., HUEY,
564 R. W., JOHNSON, B., KEE, B., LEE, M. S., MORELLI, M. P., MORRIS, V. K., OVERMAN, M. J.,
565 PARSEGHIAN, C., RAGHAV, K., WILLIS, J., WOLFF, R. A., KAWAGUCHI, Y., VAUTHEY, J.-N.,
566 SUN, R., KOPETZ, S. & SHEN, J. P. 2023. Survival improvement for patients with
567 metastatic colorectal cancer over twenty years. *npj Precision Oncology,* 7**,** 16.
568 ZHANG, X., LI, T., HAN, Y. N., GE, M., WANG, P., SUN, L., LIU, H., CAO, T., NIE, Y., FAN, D., GUO,
569 H., WU, K., ZHAO, X. & LU, Y. 2021. miR-125b Promotes Colorectal Cancer Migration and
570 Invasion by Dual-Targeting CFTR and CGN. *Cancers (Basel),* 13.
571 ZHAO, S., GUO, Y., SHENG, Q. & SHYR, Y. 2014. Advanced heat map and clustering analysis using
572 heatmap3. *Biomed Res Int,* 2014**,** 986048.
573 ZIHNI, C., MILLS, C., MATTER, K. & BALDA, M. S. 2016. Tight junctions: from simple barriers to
574 multifunctional molecular gates. *Nature Reviews Molecular Cell Biology,* 17**,** 564-580.
575

576 **9 Figure Legends**

577 **9.1 Figure 1. Expression levels of *miR-100* and *miR-125b* in CC, CC-CR and Δ*miR-***
578 ***100/miR-125b* cell lines.** (A) One of the transcription start sites within the 330kb MIR100HG
579 locus encodes a 115kb transcript that is spliced (black exons) to generate a 3kb lncRNA
580 *(MIR100HG*). *miR-100, miR-125b, let-7a* and the BLID protein are encoded in the third intron
581 of *MIR100HG*. In CC-CR cells, *MIR100HG*, *miR-100* and *miR-125b* are highly overexpressed
582 but *let-7a* is not (Lu et al., 2017). (B) CC-CR cells are a line of cetuximab-resistant cells, derived
583 from cetuximab-sensitive CC cells (Lu et al., 2017). *miR-100* and *miR-125b* are dramatically
584 overexpressed in CC-CR cells, as measured by RT-qPCR. (C) RT-qPCR analysis of *miR-100*
585 and *miR-125b* in CC-CR, Δ*miR-100*, Δ*miR-125b*, Δ*miR-100/miR-125b* cells. Fold changes were
586 determined using the ΔΔC(t) method. ** indicates p<0.005 and **** indicates p<0.0001.

587 **9.2 Figure 2. Identification of targets for *miR-100* and *miR-125b* in colorectal cancer cells.**
588 (A) Differentially expressed genes were identified by mining RNAseq data comparing CC, CC-
589 CR, Δ*miR-100*, Δ*miR-125b*, Δ*miR-100/miR-125b* cells. Venn diagram showing overlap between
590 genes upregulated in CC and knockout cell lines, mRNA targets of *miR-100* and *miR-125b* using
591 three different prediction algorithms, and association with AGO2 in CC-CR cells. (B) Heatmaps
592 were generated from the differential RNAseq data in Fig. 2A to identify potential targets
593 upregulated in CC cells (>2 fold) and knockout cells (>1.5 fold). (C) Gene Ontology analysis of
594 the targets of *miR-100* and miR-125b show enrichment in genes associated with cell migration
595 and motility. Graph was created using ShinyGO (Ge et al., 2020).

596 **9.3 Figure 3. Silencing of reporter constructs containing target 3'-UTRs for *miR-100* and**
597 ***miR-125b*.** (A) Reporter constructs were generated in which the firefly luciferase open reading
598 frame was fused to either plasmid 3'-UTR sequences (empty vector), 3'-UTR sequences
599 containing three perfect binding sites for *miR-100 or miR-125b* (100/125 vector), or 3'-UTR
600 sequences from candidate mRNA targets of *miR-100 or miR-125b* (experimental vector). (B)
601 Quantification of relative luciferase levels after transfection of the indicated constructs into CC-
602 CR cells or Δ*miR-100/miR-125b* cells. Relative firefly luciferase levels were calculated by
603 normalizing to a co-transfected internal control vector expressing Renilla luciferase. * indicates
604 p<0.05, ** indicates p< 0.01, *** indicates p<0.001, **** indicates p<0.0001.

605 **9.4 Figure 4. Expression of CGN and PTPRR are increased in cancer.** (A) Boxplot of
606 CGN (A) and PTPRR (B) expression across 72 paired tissues. Red indicates cancer samples, blue
607 indicates normal samples.

608 **9.6 Figure 5. Functional transfer of *miR-100* and *miR-125b*.** (A) RNA was collected from
609 extracellular vesicles (EVs) from CC and CC-CR cells and the levels of *miR-100* and *miR-125b*
610 were quantified by RT-qPCR. The left panel shows the fold-change enrichment of these
611 miRNAs in EVs compared to cellular levels. The right panel shows the fold-change in EV levels
612 of *miR-100* and *miR-125b* when comparing CC-CR and CC cells. (B) Transwell co-culture
613 experiments were performed with Δ*miR-100/miR-125b* recipient cells and the donor cells as
614 indicated on the X axis. RNA was collected from the recipient cells after 5 days in culture and
615 fold-changes in *miR-100* and *miR-125b* levels were determined by RT-qPCR. (C) Schematic of
616 Transwell co-culture experiments to test silencing of CGN and PTPRR luciferase reporter
617 constructs in Δ*miR-100/miR125b* recipient cells. (D) Δ*miR-100/miR-125b* recipient cells were

618 transfected with luciferase reporters (x-axis) and co-cultured with either Δ*miR-100/miR-125b*
619 (grey) or CC-CR (black) donor cells. Relative luciferase values were calculated in recipient
620 cells, normalizing as in Fig. 3. *indicates $p<0.05$, **indicates $p< 0.01$, ***indicates $p<0.001$,
621 **** indicates $p<0.0001$; ns is not significant.

622 **9.7 Figure 6. Transfer of *miR-100* and *miR-125b* decreases CGN immunofluorescence in**
623 **recipient cells.** (A) The indicated cells were fixed and immunostained with DAPI to stain nuclei
624 (blue), antibodies against F-actin (green), or antibodies against CGN (white). Merged images are
625 shown at the far right. (B) Transwell co-culture experiments were performed with Δ*miR-*
626 *100/miR-125b* recipient cells and the indicated donor cells. After 5 days, recipient cells were
627 immunostained as in Fig. 6A. Scale bar indicates 10mm.

628 **9.8 Figure 7. *miR-100* and *miR-125b* contribute to enhanced 3D growth and invasiveness.**
629 (A) The indicated cell types were plated in low adherent, spheroid cultures for 3 days before
630 transfer to growth in Type I collagen and live imaging over 5 days. (B) The increase in colony
631 area was determined by measuring the surface area of spheroids from day 0 to day 5. Surface
632 area tracing was performed using ImageJ, shown in yellow. (C) Increases in area due to colony
633 projections into the collagen (invasiveness) were calculated by measuring the total surface area
634 including projections (yellow) and subtracting the surface area of the main spheroid (red).
635 **indicates $p< 0.01$, ***indicates $p<0.001$; ns is not significant. Scale bar indicates 500mm.

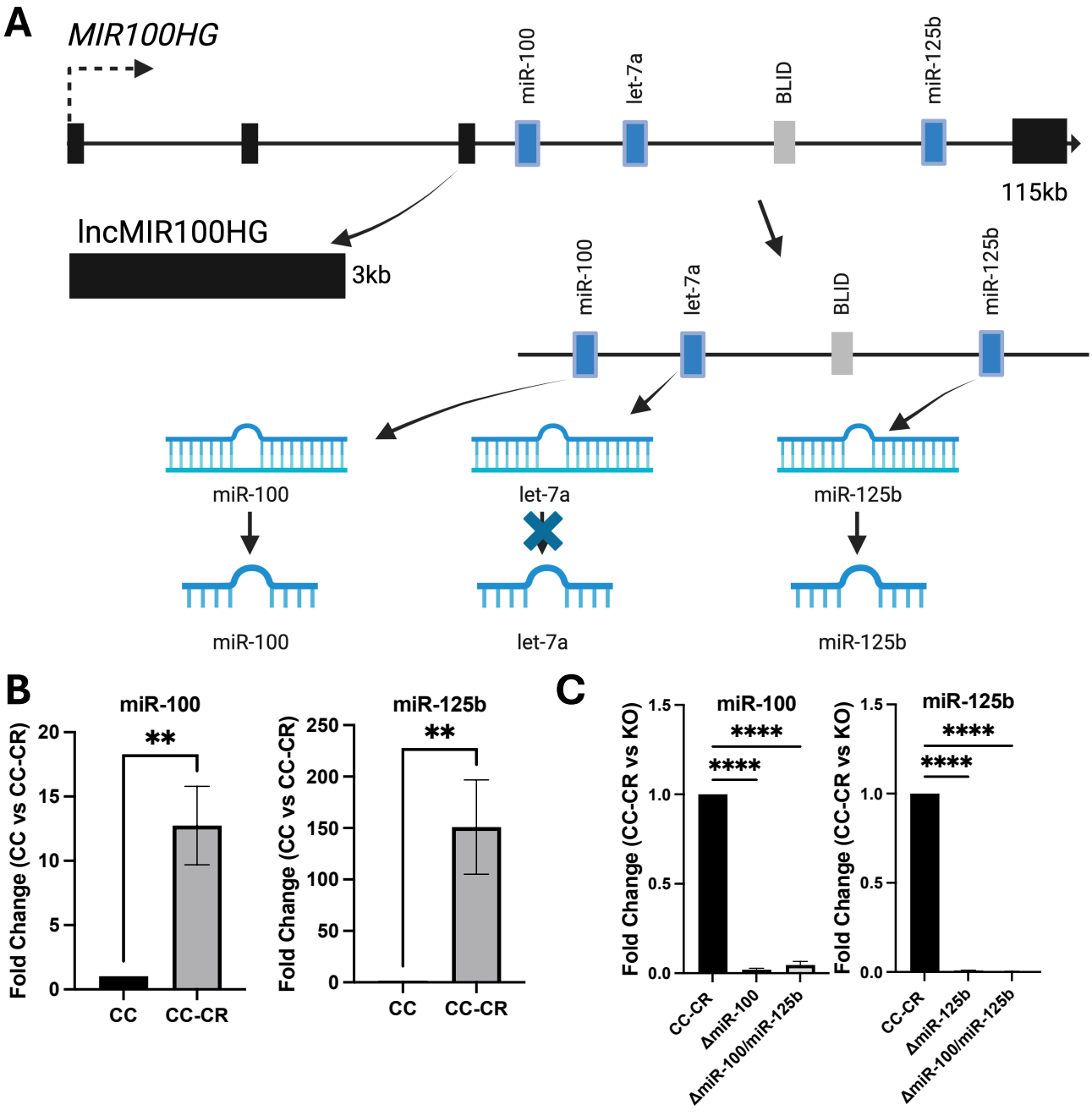
A
MIR100HG
miR-100
let-7a
BLID
miR-125b
115kb
lncMIR100HG
3kb
miR-100
let-7a
BLID
miR-125b
miR-100
let-7a
miR-125b
miR-100
let-7a
miR-125b
B
miR-100
Fold Change (CC vs CC-CR)
20
15
10
5
0
**
CC
CC-CR
miR-125b
Fold Change (CC vs CC-CR)
250
200
150
100
50
0
**
CC
CC-CR
C
miR-100
Fold Change (CC-CR vs KO)
1.5
1.0
0.5
0.0
****
****
CC-CR
ΔmiR-100
ΔmiR-100/miR-125b
miR-125b
Fold Change (CC-CR vs KO)
1.5
1.0
0.5
0.0
****
****
CC-CR
ΔmiR-125b
ΔmiR-100/miR-125b

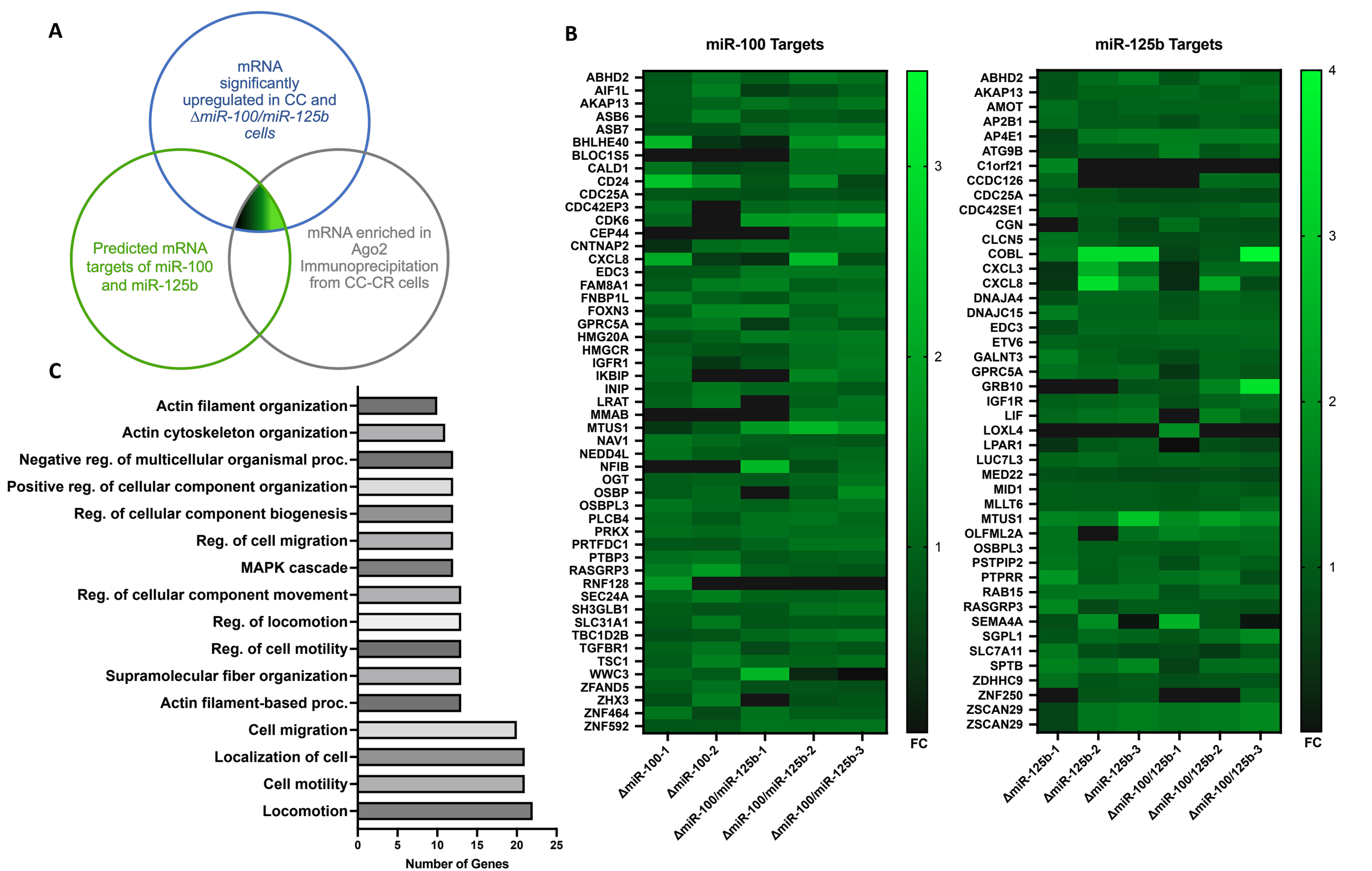
A
mRNA significantly upregulated in CC and ΔmiR-100/miR-125b cells
Predicted mRNA targets of miR-100 and miR-125b
mRNA enriched in Ago2 Immunoprecipitation from CC-CR cells
B
miR-100 Targets
ABHD2
AIF1L
AKAP13
ASB6
ASB7
BHLHE40
BLOC1S5
CALD1
CD24
CDC25A
CDC42EP3
CDK6
CEP44
CNTNAP2
CXCL8
EDC3
FAM8A1
FNBP1L
FOXN3
GPRC5A
HMG20A
HMGCR
IGFR1
IKBIP
INIP
LRAT
MMAB
MTUS1
NAV1
NEDD4L
NFIB
OGT
OSBP
OSBPL3
PLCB4
PRKX
PRTFDC1
PTBP3
RASGRP3
RNF128
SEC24A
SH3GLB1
SLC31A1
TBC1D2B
TGFBR1
TSC1
WWC3
ZFAND5
ZHX3
ZNF464
ZNF592
ΔmiR-100-1
ΔmiR-100-2
ΔmiR-100/miR-125b-1
ΔmiR-100/miR-125b-2
ΔmiR-100/miR-125b-3
FC
1
2
3
miR-125b Targets
ABHD2
AKAP13
AMOT
AP2B1
AP4E1
ATG9B
C1orf21
CCDC126
CDC25A
CDC42SE1
CGN
CLCN5
COBL
CXCL3
CXCL8
DNAJA4
DNAJC15
EDC3
ETV6
GALNT3
GPRC5A
GRB10
IGF1R
LIF
LOXL4
LPAR1
LUC7L3
MED22
MID1
MLLT6
MTUS1
OLFML2A
OSBPL3
PSTPIP2
PTPRR
RAB15
RASGRP3
SEMA4A
SGPL1
SLC7A11
SPTB
ZDHHC9
ZNF250
ZSCAN29
ZSCAN29
ΔmiR-125b-1
ΔmiR-125b-2
ΔmiR-125b-3
ΔmiR-100/125b-1
ΔmiR-100/125b-2
ΔmiR-100/125b-3
FC
1
2
3
4
C
Actin filament organization
Actin cytoskeleton organization
Negative reg. of multicellular organismal proc.
Positive reg. of cellular component organization
Reg. of cellular component biogenesis
Reg. of cell migration
MAPK cascade
Reg. of cellular component movement
Reg. of locomotion
Reg. of cell motility
Supramolecular fiber organization
Actin filament-based proc.
Cell migration
Localization of cell
Cell motility
Locomotion
0
5
10
15
20
25
Number of Genes

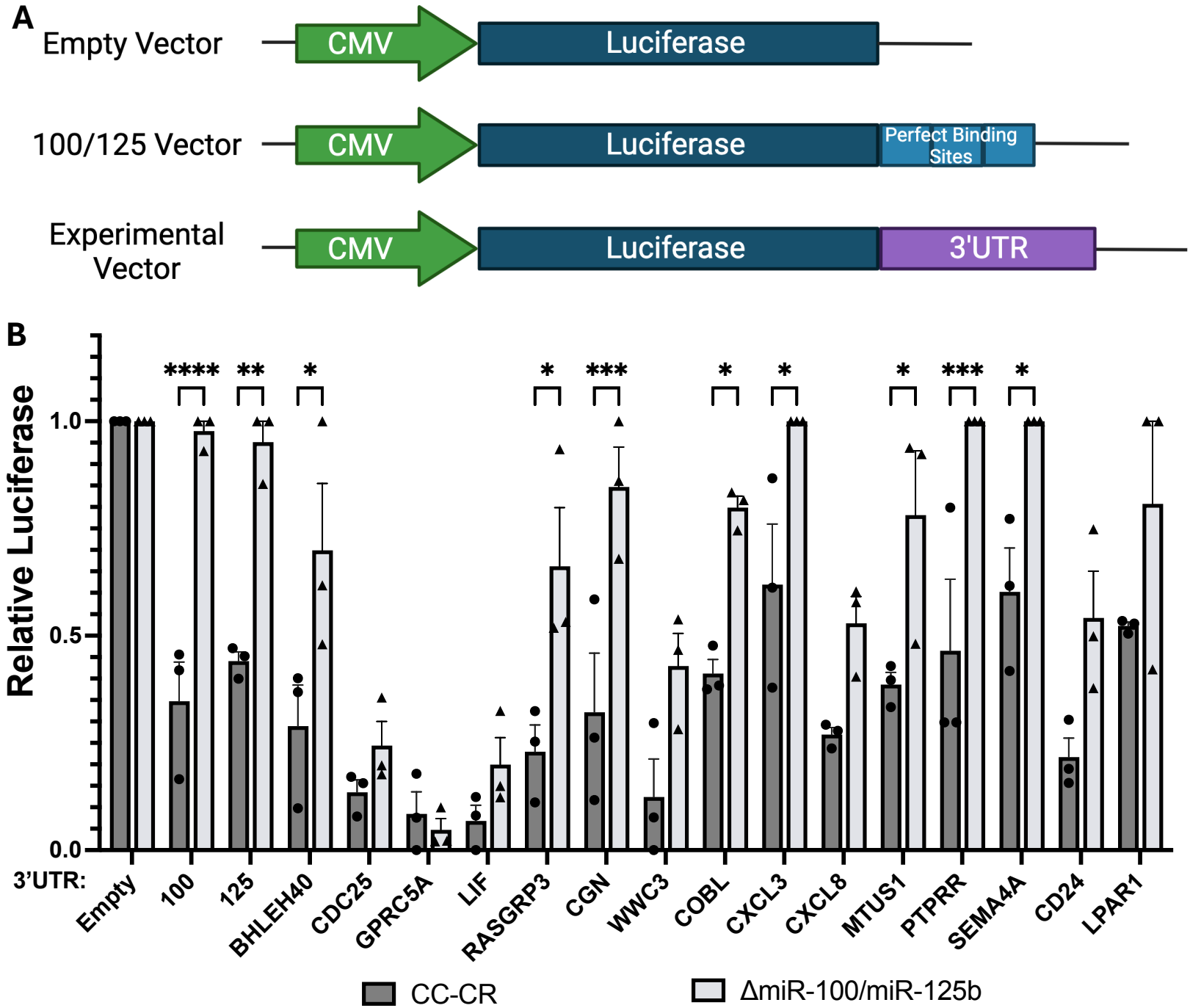
A
Empty Vector
CMV
Luciferase
100/125 Vector
CMV
Luciferase
Perfect Binding Sites
Experimental Vector
CMV
Luciferase
3'UTR
B
Relative Luciferase
1.0
0.5
0.0
****
**
*
*
***
*
*
*
***
*
3'UTR:
Empty
100
125
BHLEH40
CDC25
GPRC5A
LIF
RASGRP3
CGN
WWC3
COBL
CXCL3
CXCL8
MTUS1
PTPRR
SEMA4A
CD24
LPAR1
CC-CR
ΔmiR-100/miR-125b

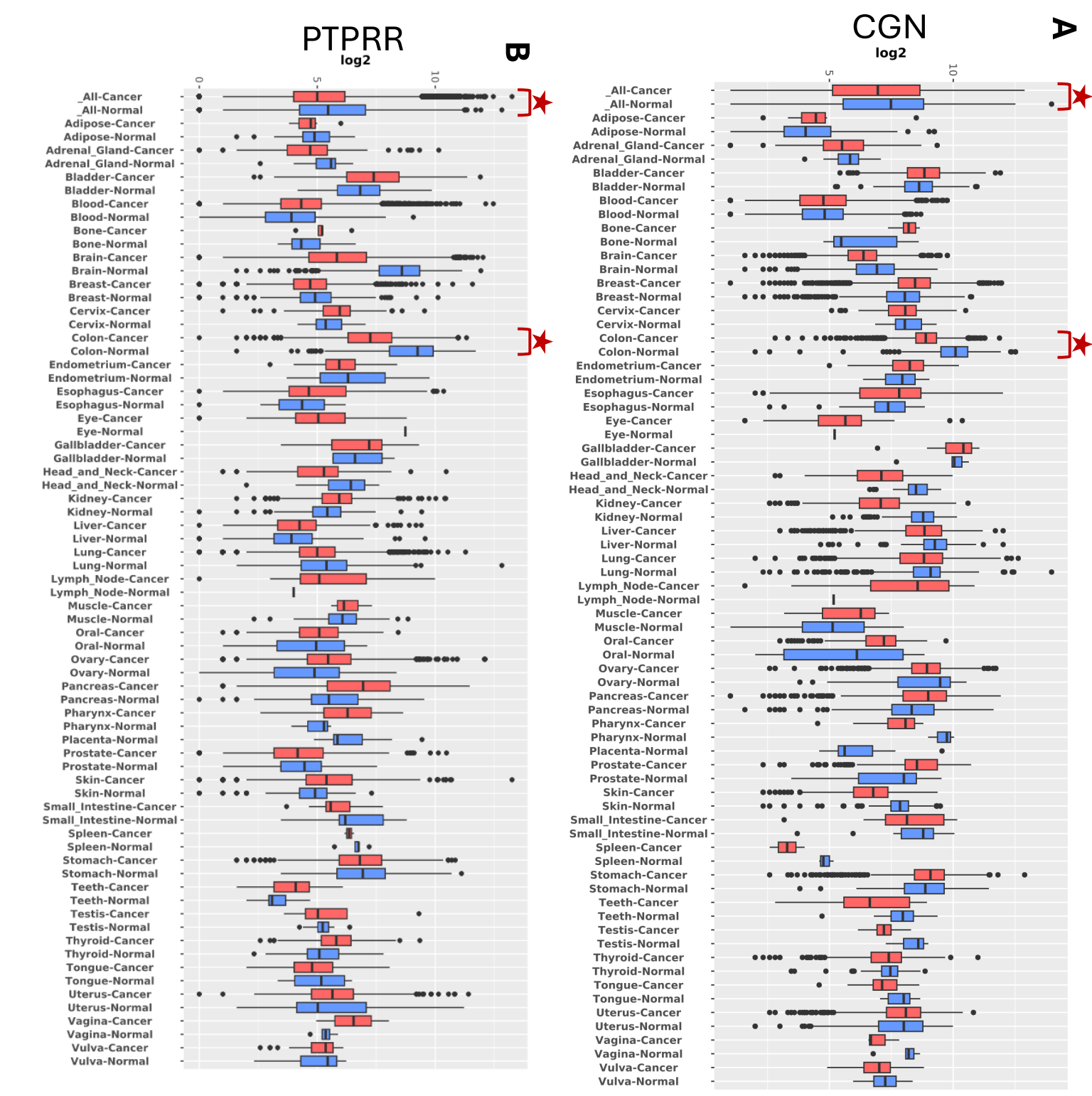
PTPRR
log2
B
0
5
10
_All-Cancer
_All-Normal
Adipose-Cancer
Adipose-Normal
Adrenal_Gland-Cancer
Adrenal_Gland-Normal
Bladder-Cancer
Bladder-Normal
Blood-Cancer
Blood-Normal
Bone-Cancer
Bone-Normal
Brain-Cancer
Brain-Normal
Breast-Cancer
Breast-Normal
Cervix-Cancer
Cervix-Normal
Colon-Cancer
Colon-Normal
Endometrium-Cancer
Endometrium-Normal
Esophagus-Cancer
Esophagus-Normal
Eye-Cancer
Eye-Normal
Gallbladder-Cancer
Gallbladder-Normal
Head_and_Neck-Cancer
Head_and_Neck-Normal
Kidney-Cancer
Kidney-Normal
Liver-Cancer
Liver-Normal
Lung-Cancer
Lung-Normal
Lymph_Node-Cancer
Lymph_Node-Normal
Muscle-Cancer
Muscle-Normal
Oral-Cancer
Oral-Normal
Ovary-Cancer
Ovary-Normal
Pancreas-Cancer
Pancreas-Normal
Pharynx-Cancer
Pharynx-Normal
Placenta-Normal
Prostate-Cancer
Prostate-Normal
Skin-Cancer
Skin-Normal
Small_Intestine-Cancer
Small_Intestine-Normal
Spleen-Cancer
Spleen-Normal
Stomach-Cancer
Stomach-Normal
Teeth-Cancer
Teeth-Normal
Testis-Cancer
Testis-Normal
Thyroid-Cancer
Thyroid-Normal
Tongue-Cancer
Tongue-Normal
Uterus-Cancer
Uterus-Normal
Vagina-Cancer
Vagina-Normal
Vulva-Cancer
Vulva-Normal
CGN
log2
A
5
10
_All-Cancer
_All-Normal
Adipose-Cancer
Adipose-Normal
Adrenal_Gland-Cancer
Adrenal_Gland-Normal
Bladder-Cancer
Bladder-Normal
Blood-Cancer
Blood-Normal
Bone-Cancer
Bone-Normal
Brain-Cancer
Brain-Normal
Breast-Cancer
Breast-Normal
Cervix-Cancer
Cervix-Normal
Colon-Cancer
Colon-Normal
Endometrium-Cancer
Endometrium-Normal
Esophagus-Cancer
Esophagus-Normal
Eye-Cancer
Eye-Normal
Gallbladder-Cancer
Gallbladder-Normal
Head_and_Neck-Cancer
Head_and_Neck-Normal
Kidney-Cancer
Kidney-Normal
Liver-Cancer
Liver-Normal
Lung-Cancer
Lung-Normal
Lymph_Node-Cancer
Lymph_Node-Normal
Muscle-Cancer
Muscle-Normal
Oral-Cancer
Oral-Normal
Ovary-Cancer
Ovary-Normal
Pancreas-Cancer
Pancreas-Normal
Pharynx-Cancer
Pharynx-Normal
Placenta-Normal
Prostate-Cancer
Prostate-Normal
Skin-Cancer
Skin-Normal
Small_Intestine-Cancer
Small_Intestine-Normal
Spleen-Cancer
Spleen-Normal
Stomach-Cancer
Stomach-Normal
Teeth-Cancer
Teeth-Normal
Testis-Cancer
Testis-Normal
Thyroid-Cancer
Thyroid-Normal
Tongue-Cancer
Tongue-Normal
Uterus-Cancer
Uterus-Normal
Vagina-Cancer
Vagina-Normal
Vulva-Cancer
Vulva-Normal

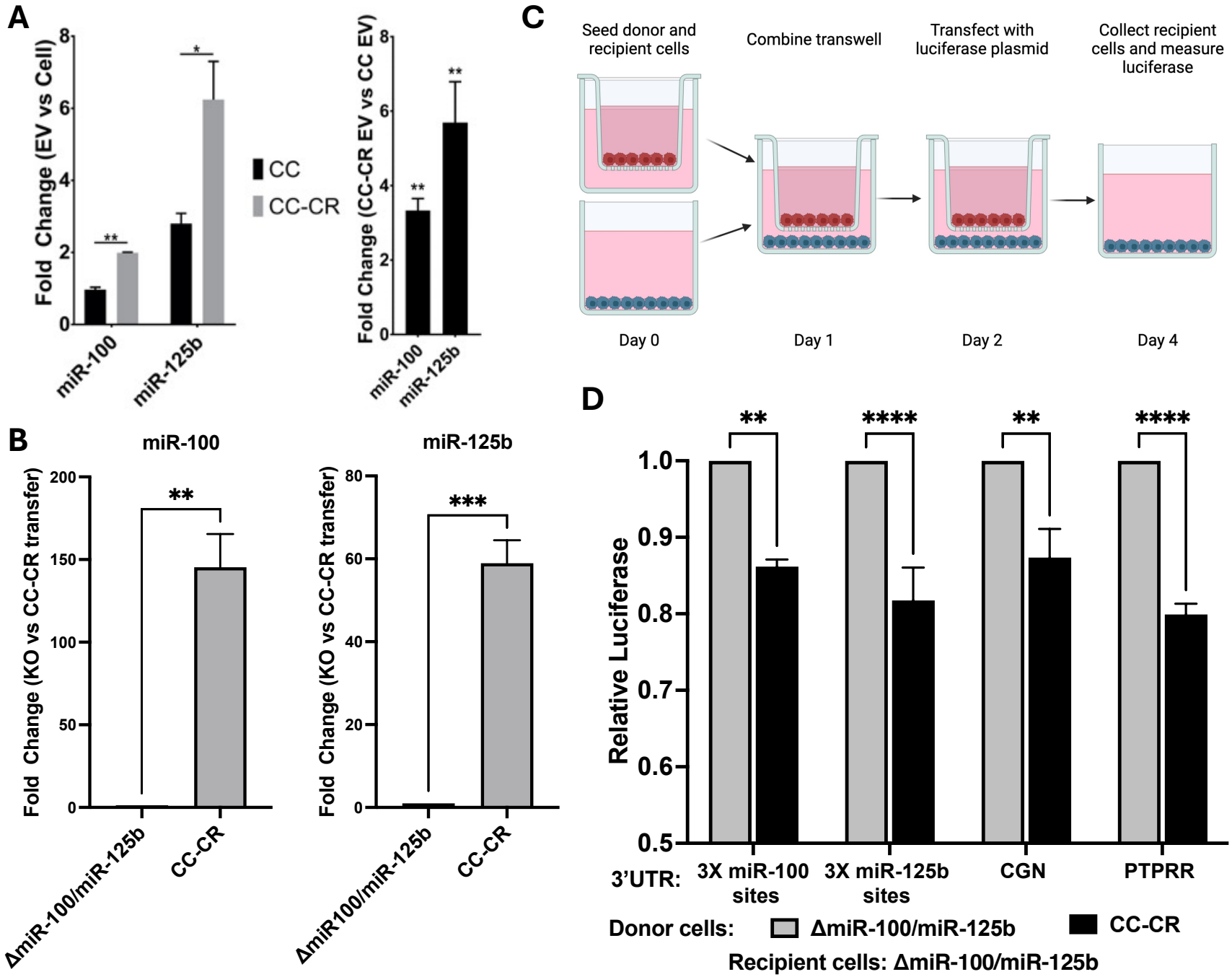
A
Fold Change (EV vs Cell)
CC
CC-CR
miR-100
miR-125b
Fold Change (CC-CR EV vs CC EV)
B
miR-100
miR-125b
Fold Change (KO vs CC-CR transfer)
ΔmiR-100/miR-125b
CC-CR
C
Seed donor and recipient cells
Combine transwell
Transfect with luciferase plasmid
Collect recipient cells and measure luciferase
Day 0
Day 1
Day 2
Day 4
D
Relative Luciferase
3'UTR:
3X miR-100 sites
3X miR-125b sites
CGN
PTPRR
Donor cells:
ΔmiR-100/miR-125b
CC-CR
Recipient cells: ΔmiR-100/miR-125b

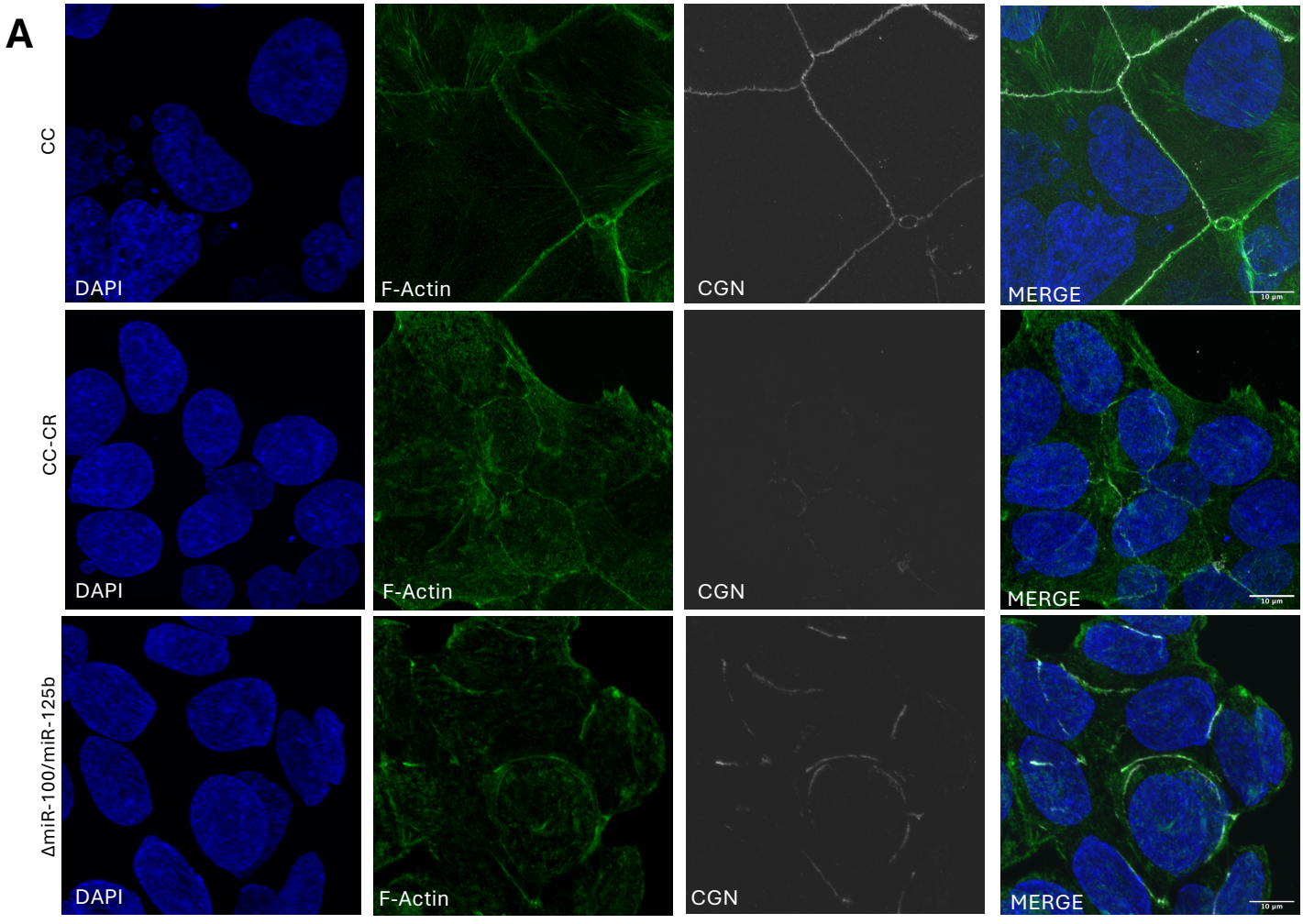
A
CC
CC-CR
ΔmiR-100/miR-125b
DAPI
F-Actin
CGN
MERGE
10 µm

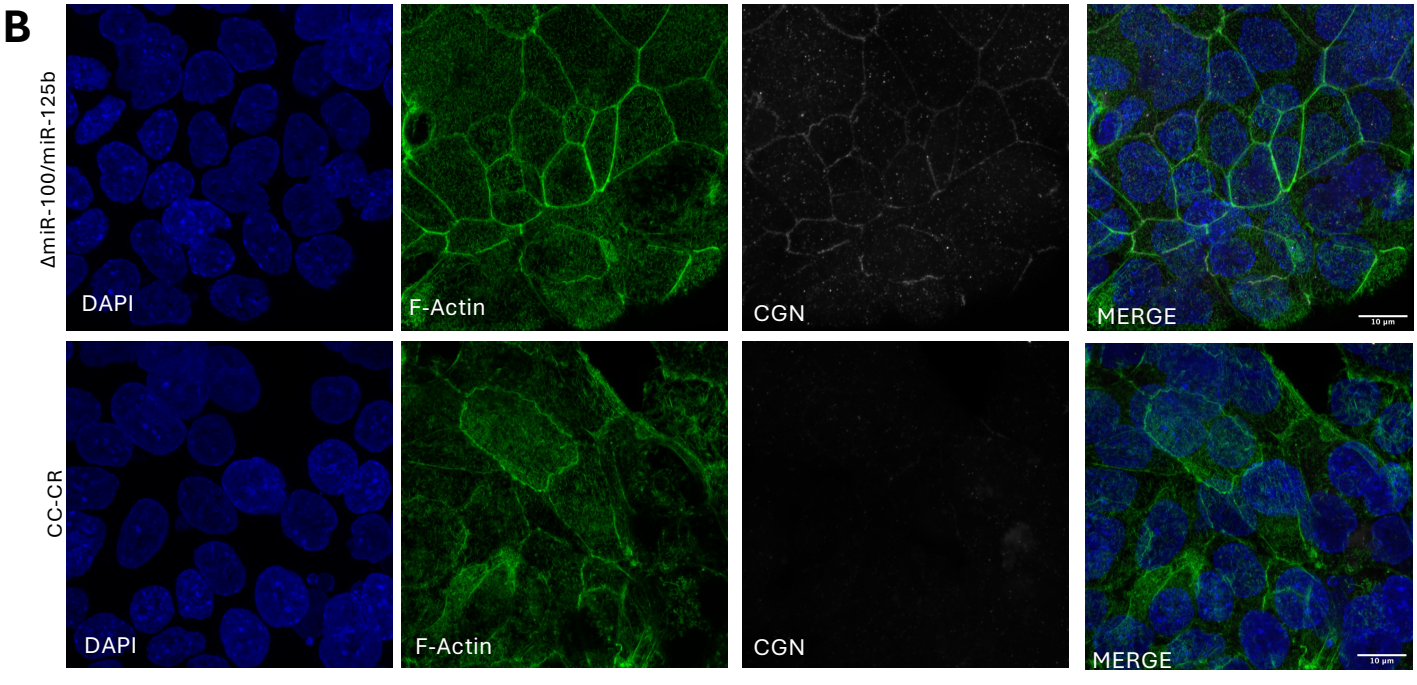
B
ΔmiR-100/miR-125b
CC-CR
DAPI
F-Actin
CGN
MERGE
10 µm

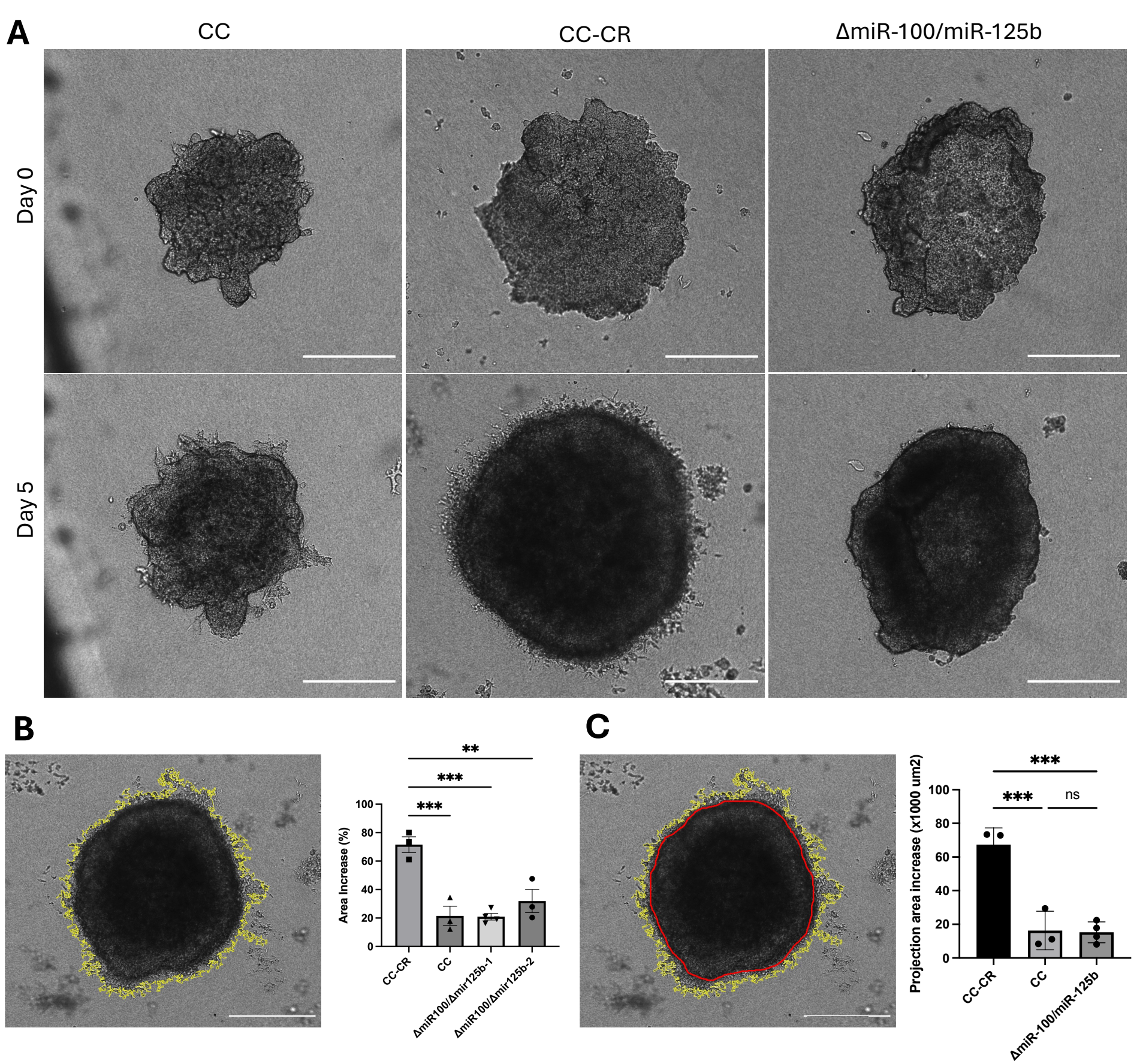
A
CC
CC-CR
ΔmiR-100/miR-125b
Day 0
Day 5
B
Area Increase (%)
100
80
60
40
20
0
**
***
***
CC-CR
CC
ΔmiR100/Δmir125b-1
ΔmiR100/Δmir125b-2
C
Projection area increase (x1000 um2)
100
80
60
40
20
0
***
***
ns
CC-CR
CC
ΔmiR-100/miR-125b